Microporous and Mesoporous Materials 227 (2016) 88–94

Contents lists available at ScienceDirect

Microporous and Mesoporous Materials

journal homepage: www.elsevier.com/locate/micromeso

Nanopore structure characterization for organic-rich shale using the non-local-density functional theory by a combination of N_2 and CO_2 adsorption

Mingming Wei, Li Zhang, Yongqiang Xiong*, Jinhua Li, Ping'an Peng

State Key Laboratory of Organic Geochemistry, Guangzhou Institute of Geochemistry, Chinese Academy of Science, Guangzhou, 510640, China

ARTICLE INFO

Article history:
Received 5 January 2016
Received in revised form
25 February 2016
Accepted 26 February 2016
Available online 3 March 2016

Keywords:
Nanopore structure
Characterization
Organic-rich shale
Low-pressure gas adsorption
NLDFT method

ABSTRACT

Low-pressure gas adsorption is widely used for pore size analysis of porous materials, and has been employed to characterize pore systems in shale. However, the complexity of shale pore structures means that different methods and models may lead to distinct interprets for adsorption data. Non-local-density functional theory (NLDFT) analysis based on N_2 and CO_2 composited adsorption isotherms is used here to investigate the pore structure of nanopores in marine organic-rich shale and compare with the results from some conventional methods in this paper. The results indicate that (1) The N_2 adsorption isotherms of organic-rich shale are a composite of Types I(b), II, and IV(a), according to the IUPAC (2015) classification of physisorption isotherms. The hysteresis loops show similar shapes to Type H2(a). Delayed capillary condensation is observed in the adsorption isotherms, and the desorption step is shifted to the lower relative pressure of ~0.45 characteristic of the cavitation mechanism, indicating ink-bottle pores with narrow necks. The CO_2 adsorption isotherms are similar to Type I(b), but appear to increase without limit when $p/p^0 = 0.03$ because of the occurrence of meso- and macropores in the shales. (2) NLDFT method based on N_2 and CO_2 composited adsorption isotherms is the most suitable and accurate method for using gas physisorption when considering the entire size distribution of nanopores, which allows a suitable range of critical pore sizes (~0.33–100 nm) to be explored.

1. Introduction

With the exploration and development of shale gas, organic-rich shales that were considered as petroleum source rocks have become key unconventional gas and oil reservoirs [1–4]. Shale gas may be stored in organic-rich shales as a combination of free, adsorbed, and dissolved gas [1,5]. Its commercial production has changed the world gas trade, and will play an increasingly important role in the future energy structure. China is the most promising country for shale growth outside North America that has so far dominated shale gas supply.

At present, shale gas evaluation and exploration in China are focused on South China, especially in and around the Sichuan Basin: for example, the lower Silurian Longmaxi marine shales, which are widespread, thick, and have a high content of total organic carbon, high thermal maturity, high quartz content, and low clay content [6–12]. The first large-scale developed shale gas field in China—the Fuling shale gas field—was found by SINOPEC in the Longmaxi Formation of the eastern Sichuan Basin in 2014. Commercial gas flows from the Longmaxi Formation of the Changning–Weiyuan Block in the southwestern Sichuan Basin have also been exploited by PetroChina.

The pores in organic-rich shales are predominantly nanometer in scale (i.e., nanopores) [13–18], and they greatly influence the ability of pore systems to store and release hydrocarbon gas and to transmit fluid to fracture networks. In nanopore structures, physisorption filling may be regarded as the primary physisorption process at the micropore scale (diameter, $D < 2$ nm), and surface coverage takes place on the walls of mesopores ($2\ \text{nm} < D < 50$ nm) or open macropores ($D > 50$ nm), which causes mono-multilayer adsorption and pore condensation [5,14,16,19–21]. Micro-scale effects such as slippage and adsorption/desorption also significantly influence the gas flow in nanopore channel systems [22]. Therefore, the investigation of nanopore systems can provide a better understanding of the gas storage and migration pathways in shales. An accurate depiction of the nanopore structure is critical for the quantification of producible resources and the evaluation of long-term production behavior.

* Corresponding author.
E-mail address: xiongyq@gig.ac.cn (Y. Xiong).

http://dx.doi.org/10.1016/j.micromeso.2016.02.050
1387-1811/

In this study, nanopores mainly include pores with widths not exceeding ~100 nm, which include micropores (<2 nm), mesopores (2–50 nm), and part of macropores (50–100 nm) [21]. Low-pressure gas adsorption is a well-established approach for the characterization of pore structures, including those in shale [12,14,16,23,24]. Nitrogen adsorption at 77 K is the standard method for pore size analysis. Nitrogen adsorption via the physisorption filling of wide micropores (i.e., $D > 0.7$ nm) [21] still occurs at very low pressures. The quadrupolar nature of the nitrogen molecule is largely responsible for its specific interaction with the functional groups on the adsorption surface, which affects the orientation of the adsorbed molecule on the surface and the micropore filling pressure. For this reason, only pores with $D >$ ~1.3 nm can be explored by N_2 adsorption at 77 K. The relatively high boiling point (273 K) and high saturation vapor pressure (~3.5 MPa) of CO_2 make studying its adsorption at 273 K an acceptable method for investigating materials with very narrow micropores (as small as 0.33 nm) [21]. On the other hand, the maximum relative pressure for measurements with CO_2 at 273 K is $p/p^0 =$ ~0.03 (corresponding to ambient pressure), which allows only pores with $D < 1$ nm to be explored. Macropores with $D > 100$ nm cannot be measured accurately with low-pressure gas adsorption of N_2 or CO_2; therefore, the combination of CO_2 and N_2 adsorption data covers a wide range of micropore to macropore sizes in the range ~0.33–100 nm, which extremely fits with the range of nanopore.

Previous studies have indicated that organic-rich shale has complex, heterogeneous nanopore structure. The pores vary widely in size (from micropores to macropores), type (e.g., interparticle and intraparticle mineral pores, intraparticle organic-matter pores, and fracture pores), and morphology (e.g., slit-shaped, ellipsoidal, spherical, and ink-bottle) [3,5,23–25]. Different methods and models have been used to evaluate surface area, pore volume, and pore size distribution (PSD) of the porous materials. For example, specific surface area is usually calculated from N_2 adsorption data by the Brunauer–Emmett–Teller (BET) [26] and *t*-plot [27–31] methods, and pore volume is generally assessed from CO_2 adsorption data by the Dubinin–Radushkevich (D–R) model [32] and from N_2 adsorption data by the Barrett–Joyner–Halenda (BJH) method [33]. Pore size distributions are mostly determined by the BJH method [8,11] and density functional theory [34] (DFT) or non-local DFT (NLDFT) [5,24,25,35,36]. However, these popular methods of characterizing pure porous materials or millimeter-to-micron scale conventional reservoirs are not normally effective for studying the complex nanopores in shale.

For instance, the BET method, established for mesoporous and macroporous materials, is not applicable to microporous adsorbents owing to the limitations of its theoretical foundation [21,37–39]. The application of the traditional BET method should be treated with caution for pore size/volume analysis owing to the existence of micropores in the organic-rich shale. Because the Langmuir equation is based on monolayer adsorption, this popular method is not suitable for the assessment of micropores, in which micropore filling is dominant. For organic-rich shale with a pore size distribution over a broad range including micropores, mesopores, and macropores, it may be impossible to separate the processes of monolayer–multilayer adsorption and micropore filling. Furthermore, capillary condensation occurs in the multilayer range of physisorption isotherms owing to the presence of mesopores. The basic limitations of the BET method have been reduced and the revised standardization of its application was proposed in the IUPAC Technical Report, 2015 [21], but that is not enough for the shale analysis.

Microporosity is often assessed by the application of the *t*-plot and α_s-plot methods. The standard multilayer thickness curve of the *t*-plot method is dependent on the application of the BET method, and thus may not be strictly applicable [29]. That makes the α_s-plot method preferred, because it does not require an evaluation of monolayer capacity, and so is more adaptable than the *t*-plot [21]. However, the α_s-plot method requires a homogeneous and absolute nonporous material as a reference material [29]. The amount adsorbed at a preselected relative pressure (generally $p/p^0 = 0.4$) of the reference material is normalized to plot the standard isotherm when using this method. It is difficult to find an eligible reference material when the sorbent is shale.

The BJH method for mesopore size analysis uses the modified Kelvin equation. Although using the Kelvin equation tends to significantly underestimate the pore size for narrow mesopores [21,20,24]. The applicability of the D–R method for microporous materials is also questionable [37,39]. DFT and NLDFT methods based on high-resolution experimental adsorption isotherms provide a reasonably reliable approach to pore size/volume analysis over the complete nanopore range [37,37,39–42]. These methods allow calculation without restriction, but it is difficult to select an accurate simplex pore shape model in the existing commercial software to interpret the heterogeneous pore structures found in shale.

The current study examined 14 core samples of black shale from the lower Silurian Longmaxi Formation in Fuling and Changning–Weiyuan, two shale gas demonstration zones. The main aims of this work are to: (1) determine the more suitable method and model for shale pore structure analysis by comparing advantages and limitations of different methods and models; (2) discuss the application of DFT- or NLDFT-based methods based on N_2 and CO_2 physisorption isotherms in the nanopore structure characterization of organic-rich shales; and (3) investigate the nanopore structure (including surface area, pore volume, and pore size distribution) of organic-rich shale of the Longmaxi Formation.

2. Experiment and methods

2.1. Samples

The studied samples were black shales from the bottom of the Longmaxi Formation collected from the JY4 drilling well in the Fuling block and the W201 drilling well in the Weiyuan–Changning block. Basic information on the samples is listed in Table 1.

2.2. Low-pressure N_2 and CO_2 adsorption

Low-pressure N_2 and CO_2 gas adsorption measurements were conducted on a Micromeritics ASAP-2460 Accelerated Surface Area and Porosimetry System. Samples were crushed to 60–120 mesh size. Subsequent automatic degassing at 110 °C for ~12 h (Micromeritics VacPrep 061 degasser) removed the gas, free water, and any other possible hydrocarbons. The equilibrium interval (i.e., the time during which the pressure must remain stable within a small range) was 30 s for N_2 and 45 s for CO_2. The relative pressure (p/p^0) was 0.005–0.995 for N_2 adsorption and 0.00006–0.03 for CO_2 adsorption. During the CO_2 adsorption measurements, the free spaces were tested separately and input manually.

The N_2 and CO_2 adsorption isotherms were automatically generated by the instrument. The surface area, pore volume, and PSDs were then calculated based on various adsorption theories.

2.3. Application of the BET method

The BET method is the most widely used procedure for assessing the special surface area of powders and porous solids [37–39]. The BET equation (Eq. (1)) is usually applied in the linear form:

Table 1
Basic information on the shale samples.

Sample ID	Sampling location	Formation	Depth (m)	TOC (%)	Sample ID	Sampling location	Formation	Depth (m)	TOC (%)
JY4-2	Fuling shale	Longmaxi	2540	0.87	W201-1	Changning-Weiyuan	Longmaxi	1504	0.93
JY4-5	gas		2550	1.34	W201-12	shale gas		1514	1.79
JY4-9	demonstration zone		2559	2.44	W201-23	demonstration zone		1524	2.97
JY4-12			2565	3.25	W201-27			1528	1.63
JY4-14			2573	2.20	W201-30			1529	4.17
JY4-16			2578	3.01	W201-32			1533	2.89
JY4-19			2587	3.50	W201-43			1543	5.07

$$\frac{p/p^0}{n(1-p/p^0)} = \frac{1}{n_m C} + \frac{C-1}{n_m C}\left(p/p^0\right), \quad (1)$$

where n is the specific amount adsorbed at the relative pressure p/p^0, n_m is the specific monolayer capacity, and the parameter C is exponentially related to the energy of monolayer adsorption.

Owing to the limitations of BET theoretical foundation, conventional BET equation cannot be applied without extreme caution in microporous materials, which can be applied in the part of mesopores without capillary condensation in the multilayer range of physisorption isotherms. For this reason, some application criteria should be established for the application of the BET method to shale study. In the present study, comparing the experimental data for the shale samples with the classic BET equation data clearly shows that the equation only applies to low relative pressure and significantly overestimates the adsorption at relative pressures higher than 0.15. The equation is often restricted within the p/p^0 range of ~0.05–0.30. Therefore, for BET analysis the p/p^0 value of porous shale samples should be within the range ~0.05–0.15. This agrees with the selection criteria of Rouquerol et al. [38] and Thommes et al. [21] for microporous adsorbents, which allow one to avoid any subjectivity in evaluating the BET monolayer capacity. The application of the BET method for shales is based on the following main criteria: (1) that p/p^0 lies within the range of ~0.05–0.15; (2) that the term $(1 - p/p^0)$ continuously increases with p/p^0, and 5–8 points should be selected; and (3) that the quantity C is positive—preferably as small as possible—and the correlation coefficient is greater than 0.9999.

Finally, the BET areas are obtained in the range of ~1.3–100 nm (Table 2), an apparent surface area that should not be treated as a realistic probe-accessible surface area, especially for micropores.

2.4. Application of the t-plot method

The *t*-plot method is more likely to be used for routine analysis comparing with α_s-plot method. The *t*-plot method commonly uses the Harkins–Jura thickness equation [30,43] (Eq. (2)). The thickness (*t* value) should be within the range of ~0.35–0.45 nm when the p/p^0 value is within the same range of ~0.05–0.15 as for the BET method. The thickness range may not be strictly applicable, so we select a thickness range of 0.6–0.8 nm to obtain the microporosity data (Table 2) and compare the results with other methods and models.

$$t = \left[\frac{0.1399}{0.034 - \log\left(p/p^0\right)}\right]^{1/2}, \quad (2)$$

where *t* is the multilayer thickness of adsorbed layer at the relative pressure p/p^0.

2.5. BJH method

Though the pore size for narrow mesopores always be underestimated by the BJH method, the BJH method may still be useful for routine work. The BJH surface areas ($S_{mes\text{-}mac}$(BJH)) and pore volumes ($V_{mes\text{-}mac}$(BJH)) listed in Table 2 are within the pore-size range of 2–100 nm. The BET micropore surface areas (S_{mic}(BET)) (Table 2) then obtained by subtracting the BJH areas from the BET areas refer to the surface area of micropores with sizes within the range of 1.3–2 nm.

2.6. DFT and NLDFT methods

DFT- and NLDFT-based methods for pore size/volume analysis of nanoporous materials are now available for many adsorption systems [37,39,40]. They allow the calculation of a series of theoretical isotherms without restriction (e.g., p/p^0) for a particular adsorptive/adsorbent pair. Pores within the range of ~0.33–1 nm can be explored with CO_2 at 273 K, and pores within the range of ~1.3–100 nm can be explored with N_2 at 77 K using DFT. The N_2 and CO_2 data can be automatically fitted using NLDFT via measurement by Micromeritics ASAP-2460. Overall, pores of ~0.33–100 nm can be explored for nanopore analysis. Therefore, the composite of N_2 and CO_2 by NLDFT provides a reasonably reliable analysis of the whole nanopore size distribution. The parameters of nanopore structure and critical nanopore ranges obtained by DFT and NLDFT are listed in Table 3.

3. Results and discussion

3.1. Adsorption isotherms

Adsorption isotherms and hysteresis loops can reveal the pore shape, size, and volume of porous materials [29]. Fig. 1 presents the N_2 isotherms of a few typical organic-rich shale samples from the Sichuan Basin, China, which are similar to those of the Perth and Canning shales [25], and mudstone from the Western Canada Basin.[55] However, different type classifications were suggested for these N_2 adsorption isotherms. For example, the Perth, Canning, and Western Canada samples showed isotherms of Type I [36], II [24], and IV [25], respectively, according to the IUPAC classification of adsorption isotherms and hysteresis loops [21]. Here, we suggest that the N_2 isotherm is a composite of Types I(b), II, and IV(a). The steep uptake (micropore filling) at very low relative pressures, Point B (the beginning of monolayer-multilayer adsorption on the mesopore walls), hysteresis loop (capillary condensation), and sharp uptake (unrestricted monolayer-multilayer adsorption) at a relative pressure close to unity (i.e., $p/p^0 = 0.95$) indicate that these shales possess a hierarchical pore structure containing a broad range of pore sizes from micropores to macropores. A significant amount of adsorption at low relative pressure (i.e., $p/p^0 < 0.05$) is indicative of microporosity.

Table 2
Pore structure parameters obtained by the BET, BJH, and *t*-plot methods.

Sample ID	BET method		BJH method		*t*-plot method with H–J thickness equation		
	S_{total}(BET) (m^2/g)	S_{mic}(BET) (m^2/g)	$S_{mes\text{-}mac}$(BJH) (m^2/g)	$V_{mes\text{-}mac}$(BJH) (10^{-3} cm^3/g)	S_{mic}(*t*-plot) (m^2/g)	S_{ext}(*t*-plot) (m^2/g)	V_{mic}(*t*-plot) (10^{-3} cm^3/g)
	Range (nm)		Range (nm)		Range (nm)		
	1.3–100	1.3–2	2–100		1.3–2	2–100	1.3–2
JY4-2	17.03	8.26	8.77	19.07	8.00	9.02	3.92
JY4-5	15.44	8.84	6.60	13.10	8.88	6.56	4.25
JY4-9	20.64	11.10	9.54	16.11	11.60	9.04	5.49
JY4-12	26.11	15.39	10.72	24.67	15.12	11.00	7.05
JY4-14	20.34	11.57	8.77	16.51	12.13	8.21	5.67
JY4-16	22.59	12.93	9.66	16.00	13.16	9.43	6.06
JY4-19	24.24	13.41	10.83	22.20	13.69	10.55	6.28
W201-1	19.83	7.22	12.61	29.41	7.11	12.72	3.56
W201-12	20.20	9.42	10.78	23.90	9.70	10.49	4.66
W201-23	22.41	11.26	11.15	23.86	11.92	10.50	5.70
W201-27	16.14	6.39	9.75	22.21	6.42	9.72	3.17
W201-30	33.40	17.82	15.58	26.08	18.70	14.70	8.83
W201-32	22.56	9.73	12.82	27.92	10.54	12.02	5.29
W201-43	26.68	18.53	8.15	10.57	19.15	7.53	8.68

Table 3
Pore structure parameters obtained by the DFT and NLDFT methods.

Sample ID	DFT Model with N_2						Composited N_2 and CO_2 NLDFT Model					
	Surface areas (m^2/g)			Pore volumes (10^{-3} cm^3/g)			Surface areas (m^2/g)			Pore volumes (10^{-3} cm^3/g)		
	S_{mic}(DFT)	S_{mes}(DFT)	S_{mac}(DFT)	V_{mic}(DFT)	V_{mes}(DFT)	V_{mac}(DFT)	S_{mic}(NLDFT)	S_{mes}(NLDFT)	S_{mac}(NLDFT)	V_{mic}(NLDFT)	V_{mes}(NLDFT)	V_{mac}(NLDFT)
	Range (nm)			Range (nm)			Range (nm)			Range (nm)		
	1.3–2	2–50	50–100	1.3–2	2–50	50–100	0.33–2	2–50	50–100	0.33–2	2–50	50–100
JY4-2	1.31	1.41	0.03	0.91	6.35	1.16	14.43	4.27	0.06	4.63	17.84	2.25
JY4-5	1.61	1.70	0.02	1.15	5.17	0.64	13.78	3.04	0.02	4.66	10.72	0.90
JY4-9	2.12	1.77	0.03	1.50	5.41	0.87	18.44	4.15	0.04	6.17	15.23	1.25
JY4-12	2.55	1.51	0.05	1.79	5.18	1.56	23.96	5.03	0.06	7.94	20.16	2.03
JY4-14	2.34	2.44	0.04	1.69	7.14	1.36	19.05	3.70	0.04	6.28	12.68	1.45
JY4-16	2.88	2.10	0.02	2.04	6.30	0.65	20.82	4.19	0.03	6.97	14.76	1.18
JY4-19	2.78	2.16	0.04	1.99	7.03	1.18	22.08	4.77	0.05	7.34	17.84	1.67
W201-1	1.28	2.08	0.06	0.90	8.98	2.01	14.85	5.72	0.06	5.05	24.28	2.11
W201-12	1.89	1.35	0.05	1.29	6.81	1.83	16.81	4.91	0.09	5.62	21.58	3.79
W201-23	2.69	1.26	0.05	1.86	6.25	1.57	20.48	5.04	0.09	6.51	21.83	3.71
W201-27	1.27	1.50	0.06	0.88	7.77	2.16	12.77	4.55	0.08	4.21	20.48	3.46
W201-30	4.32	3.68	0.04	3.06	11.29	1.38	29.33	6.77	0.06	10.01	24.16	2.13
W201-32	1.88	1.93	0.08	1.29	9.43	2.70	20.25	5.86	0.12	6.22	25.49	4.73
W201-43	3.58	2.22	0.01	2.55	5.07	0.33	26.81	3.20	0.02	9.08	9.06	0.61

Hysteresis generally associated with capillary condensation occurs when the pore width exceeds a certain critical width, and it always occurs for pores wider than ~4 nm [37,40,41]. The hysteresis loop in Fig. 1 appears similar to Type H2(a). Delayed capillary condensation is observed in the adsorption isotherms, while the desorption step is shifted to a lower relative pressure of ~0.45 characteristic of the cavitation mechanism, indicative of ink-bottle pores with narrow necks.

The Type I(b) CO_2 adsorption isotherms in Fig. 2 indicate microporous materials with a broad pore-size distribution including wider micropores and possibly narrow mesopores (<~2.5 nm). The isotherms are concave to the p/p^0 axis, and the amount adsorbed appears to increase without limit when $p/p^0 = 0.03$ because of the meso- and macropores in the shale.

3.2. Surface areas analysis

The physisorption isotherm is the only result measured using low-pressure gas adsorption, all the parameters characterizing pore systems are obtained using various methods and models based on different principles and assumptions. If the principles and applicable conditions of the methods are not considered, the obtained parameters are meaningless and inaccurate. Therefore, the appropriate choice of method is crucial to the accurate characterization of a shale nanopore system from its physisorption isotherm.

DFT- or NLDFT-based methods have been developed for the accurate and comprehensive analysis of pore structures for various adsorbent systems and pore geometries (e.g., cylindrical, slit, spherical, or hybrid). The determination of pore structure parameters from DFT- or NLDFT-based methods and other popular methods is discussed below.

The total specific surface areas calculated from the adsorption isotherms using the BET method and composited N_2 and CO_2 NLDFT are presented in Tables 2 and 3, respectively. The total specific surface areas obtained by the BET method (S_{total}(BET)) for the 14 samples range from 15.44 to 33.40 m^2/g with a mean of 21.97 m^2/g. The NLDFT total specific surface areas (S_{total}(NLDFT)) (range 16.84–36.16 m^2/g, mean 24.27 m^2/g) are slightly higher than the BET areas, because the probed pore range (~0.33–2 nm) in the NLDFT method is greater than the analysis range (~1.3–2 nm) of BET.

The micropore surface areas (S_{mic}(*t*-plot)) and non-micropore surface areas (S_{ext}(*t*-plot)) calculated by the *t*-plot method and S_{mic}(BET) obtained by subtracting the BJH areas from the BET areas

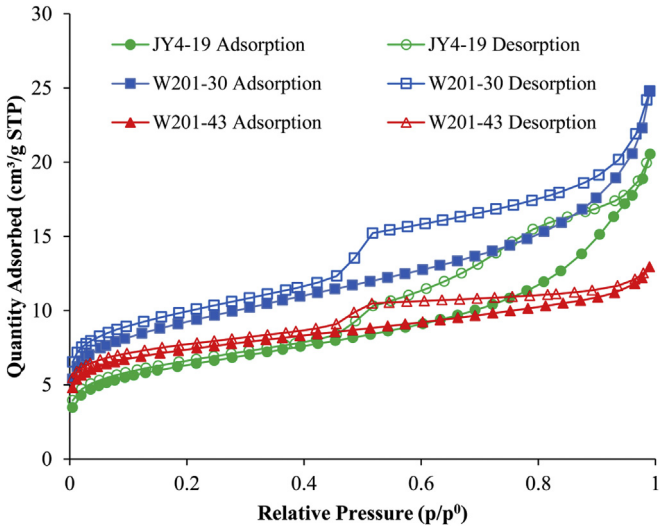

Fig. 1. N_2 isotherms of typical organic-rich shale samples from the Sichuan Basin, China.

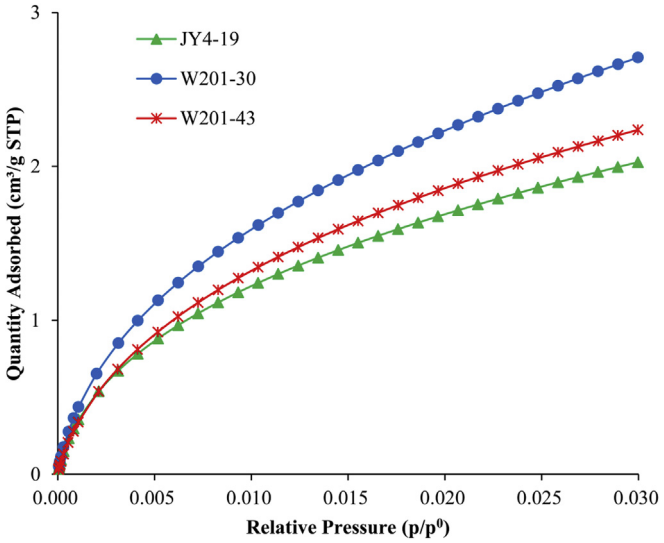

Fig. 2. CO_2 isotherms of typical organic-rich shale samples from the Sichuan Basin, China.

are presented in Table 2. The specific surface areas of micropores and meso- and macropores calculated by DFT (S_{mic}(DFT) and $S_{mes\text{-}mac}$(DFT)) and by composited N_2 and CO_2 NLDFT (S_{mic}(NLDFT) and $S_{mes\text{-}mac}$(NLDFT)) are listed in Table 3. Micropores are the major contributor to the specific surface areas. The S_{mic}(BET) (range 6.39–18.53 m^2/g, mean 11.56 m^2/g) and the S_{mic}(*t*-plot) (range 6.42–19.15 m^2/g, mean 11.87 m^2/g) values are similar to each other. However, the S_{mic}(NLDFT) (range 12.77–29.33 m^2/g, mean 19.56 m^2/g) values are much larger, as the pores within the range of ~0.33–2 nm can be explored by the composited N_2 and CO_2 NLDFT method. The $S_{mes\text{-}mac}$(NLDFT) values (range 3.06–6.83 m^2/g, mean 4.71 m^2/g) are slightly lower than the S_{ext}(*t*-plot) values (range 6.56–14.7 m^2/g, mean 10.11 m^2/g), which means that S_{ext}(*t*-plot) may contain the surface areas of some interparticle pores and pores larger than 100 nm. Both S_{mic}(DFT) (range 1.27–4.32 m^2/g, mean 2.32 m^2/g) and $S_{mes\text{-}mac}$(DFT) (range 1.3–3.72 m^2/g, mean 1.98 m^2/g) are smaller than the respective values calculated by other methods.

The correlations of the total specific surface areas obtained by the BET method and composited N_2 and CO_2 NLDFT are generally similar and linearly related (Fig. 3a), indicating that both methods (the former specifically with definite criteria) are suitable for analysis of the total specific surface area. The correlations of micropore surface areas from the deduction of BET and BJH areas and from the *t*-plot method with the Harkins–Jura thickness equation are plotted in Fig. 3b. Both micropore surface areas appear very similar and linearly related, which further supports the proposal that both the BET method and the *t*-plot method are intrinsically identical when the proper thickness model is used in the latter. The micropore surface areas from the *t*-plot, DFT, and NLDFT methods are similar and linearly related (Fig. 3c), suggesting their suitability for analyses of micropore surface area. However, the meso- and macropore surface areas from DFT deviate significantly from the corresponding data obtained by NLDFT (Fig. 3e), which means that DFT is not ideally suited for mesopore and macropore surface area analysis.

Similar conclusions can be made based on the SPSS Reliability Statistics. The value of Cronbach's Alpha based on standardized items of micropore surface areas obtained from the *t*-plot, DFT, and NLDFT methods is 0.94, which indicates good statistical reliability of the micropore surface areas obtained using the three methods. However, the Cronbach's Alpha based on standardized items of mesopore and macropore surface areas obtained from the BJH and DFT methods is 0.725, which means that the meso- and macropore surface areas obtained from these methods need to be revised.

To sum up, the composited N_2 and CO_2 NLDFT method is the most suitable method for the analysis of specific surface area, including micro-, meso-, and macropore surface area, and total area.

3.3. Pore volumes analysis

The micropore volumes calculated by the *t*-plot (V_{mic}(*t*-plot)), DFT (V_{mic}(DFT)), and composited N_2 and CO_2 NLDFT (V_{mic}(NLDFT)) methods are presented in Tables 2 and 3, respectively. The V_{mic}(*t*-plot) value (range 3.17 × 10^{-3} to 8.83 × 10^{-3} cm^3/g, mean 5.62 × 10^{-3} cm^3/g) is slightly smaller than the V_{mic}(NLDFT) value (range 4.21 × 10^{-3} to 10.01 × 10^{-3} cm^3/g, mean 6.48 × 10^{-3} cm^3/g), because only the pores of size ~1.3–2 nm can be explored using the *t*-plot method.

The BJH volume ($V_{mes\text{-}mac}$(BJH)) and the meso- and macropore volumes calculated by DFT ($V_{mes\text{-}mac}$(DFT)) and by composited N_2 and CO_2 NLDFT ($V_{mes\text{-}mac}$(NLDFT)) are presented in Tables 2 and 3, respectively. The range of $V_{mes\text{-}mac}$(BJH) values is 10.57 × 10^{-3} to 29.41 × 10^{-3} cm^3/g (mean 20.83 × 10^{-3} cm^3/g). The range of $V_{mes\text{-}mac}$(NLDFT) values is 9.66 × 10^{-3} to 30.22 × 10^{-3} cm^3/g (mean 20.53 × 10^{-3} cm^3/g), and the mesopores are the major contributor to the pore volumes. The values from DFT (i.e., V_{mic}(DFT), range 0.88 × 10^{-3} to 3.06 × 10^{-3} cm^3/g, mean 1.64 × 10^{-3} cm^3/g; $V_{mes\text{-}mac}$(DFT), range 5.4 × 10^{-3} to 12.67 × 10^{-3} cm^3/g, mean 8.4 × 10^{-3} cm^3/g) are both smaller than those calculated by other methods.

The micropore volumes from the *t*-plot, DFT, and NLDFT methods are mostly similar to each other and linearly related (Fig. 3d), which indicates the suitability of these methods for micropore volumes analysis. However, the meso- and macropore volumes obtained from DFT deviate significantly from the corresponding data from NLDFT (Fig. 3f), indicating that DFT is not ideally suited for mesopore and macropore volume analysis.

The value of Cronbach's Alpha, from the SPSS Reliability Statistics, based on standardized items of micropore volumes obtained

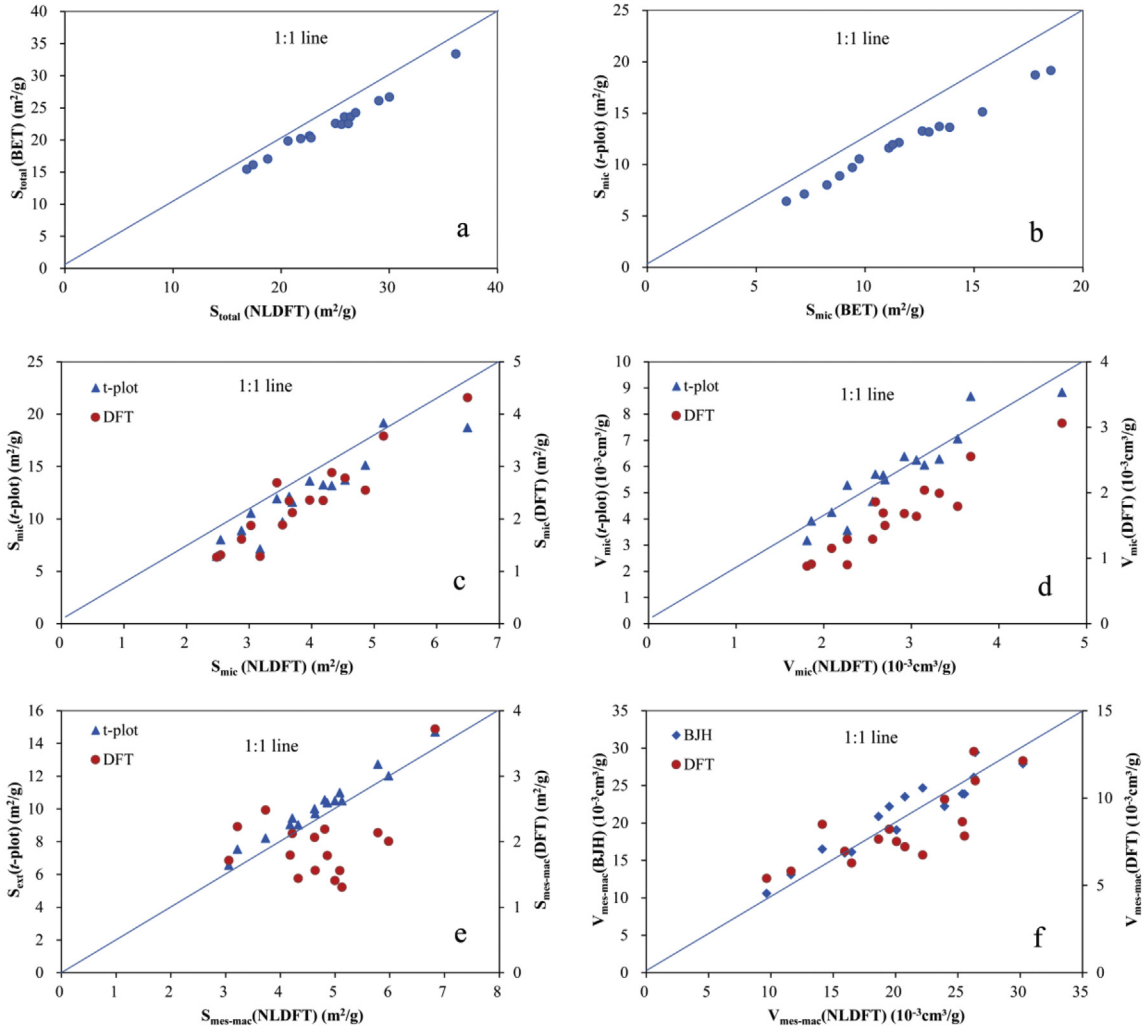

Fig. 3. Comparisons of results obtained from various analysis methods.

from the *t*-plot, DFT, and NLDFT methods is 0.979, which indicates statistically good reliability of the three methods. However, the value of Cronbach's Alpha based on standardized items of meso-pore and macropore volumes obtained from the BJH and DFT methods is 0.740, which means that the meso- and macropore volumes obtained from these methods need be revised. Therefore, the results of rigorous data processing indicate that the N_2 and CO_2 composited NLDFT method is reliable and accurate.

3.4. NLDFT pore size distributions (PSDs)

A plot of dV/dlog(D) versus D (pore diameter) for N_2 and CO_2 is commonly used to illustrate the pore size distribution [8,11,14,16,24,44], and is used to compare the relative pore volumes between any pore size ranges, because the "visual area" under the curve of dV/dlog(D) is proportional to the real volume.

The combination of CO_2 and N_2 adsorption data can enable pore size analysis for micro-to macroporosity up to a limit of ~100 nm [24]. Fig. 4 presents the pore size distributions of two typical shale samples, as automatically calculated and fitted by the ASAP-2460 analyzer based on the N_2 and CO_2 adsorption data using the NLDFT method. In dV/dlogD vs. pore diameter plots, the CO_2 and N_2 curves start and end, respectively, at 2 nm in a near seamless transition (Fig. 4). The two curves also indicate multi-modal PSDs in the shale pore structure.

From the above, it is clear that the most suitable critical range of ~0.33–100 nm can be explored by the composited N_2 and CO_2 NLDFT method, which shows high reliability and accuracy over the entire range of nanopore sizes. Therefore, data analyzed using this method will be discussed in detail for the entire nanopore size range in a following study.

4. Conclusion

Low-pressure N_2 and CO_2 adsorption tests explored the nano-pore structures of organic-rich shale from drillcore samples. The main conclusions are as follows.

(1) Methodology principle analysis, comparisons, and SPSS reliability statistics of the experimental results indicate that the composited N_2 and CO_2 NLDFT method is the most suitable approach for gas physisorption data analysis in shale research. This method allows the most suitable detection range (~0.33–100 nm) and has high reliability and accuracy over the entire nanopore size range.

(2) The N_2 physisorption isotherms obtained in this study are a composite of Types I(b), II, and IV(a), according to the IUPAC

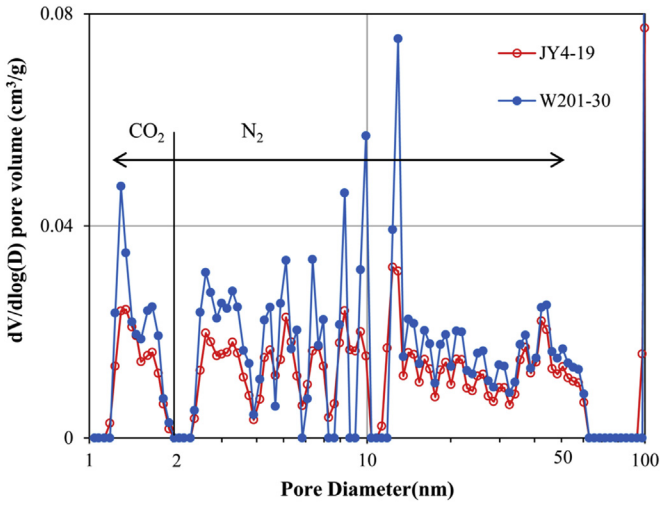

Fig. 4. Plot of dV/dlog(D) versus D for the pore size distribution of two typical organic-rich shale samples from the Sichuan Basin, China, obtained by the NLDFT method based on N_2 and CO_2 adsorption isotherms. Arrows indicate the range of pore sizes covered by N_2 and CO_2 adsorption.

(2015) classification. The shapes of the hysteresis loops appear similar to Type H2(a), and are attributed either to pore-blocking in the case of narrow pore necks (e.g., ink-bottle pores) or to cavitation-induced evaporation. The CO_2 physisorption isotherms appear similar to Type I(b), but increase without limit when $p/p^0 = 0.03$ because of the meso- and macropores in shales.

(3) Micropore surface area and mesopore volume are the most important parameters of nanopore structure in shale, because the amount of adsorbed gas in shale depends mainly on the micropore surface area, and the content of free gas is determined by meso- and macropore volume, especially the mesopore volume. The studied samples have micropore surface areas of 12.77–29.33 m^2/g (mean 19.56 m^2/g) and mesopore volumes of 9.66 $\times$ 10^{-3} to 30.22 $\times$ 10^{-3} cm^3/g (mean 20.53 $\times$ 10^{-3} cm^3/g).

Acknowledgements

This work was financially supported by Special Fund for Strategic Priority Research Program of the Chinese Academy of Sciences (Class B) (Grant No. XDB10010500) and the Chinese Ministry of Land and Resources (Grant No. Zi[2014]03-030-003). We are grateful to editor Kenneth Balkus and two anonymous reviewers for their instructive comments and suggestions that significantly help clarify this manuscript. This is contribution No. IS-2197 from GIGCAS.

References

[1] J.B. Curtis, AAPG Bull. 86 (11) (2002) 1921–1938.
[2] D.M. Jarvie, R.J. Hill, T.E. Ruble, R.M. Pollastro, AAPG Bull. 91 (2007) 475–499.
[3] R.G. Loucks, R.M. Reed, S.C. Ruppel, D.M. Jarvie, J. Sediment. Res. 79 (2009) 848–861.
[4] J.Q. Tan, B. Horsfield, R. Fink, B. Krooss, H. Schulz, E. Rybacki, J.C. Zhang, C.J. Boreham, G. Graas, B.A. Tocher, Energy Fuels 28 (2014) 2322–2342.
[5] D.J. Ross, R.M. Bustin, Mar. Petrol. Geol. 26 (6) (2009) 916–927.
[6] C. Zou, D. Dong, S. Wang, J. Li, X. Li, Y. Wang, D. Li, K. Cheng, Petrol. Explor. Dev. 37 (2010) 641–653.
[7] S.B. Han, J.C. Zhang, Y.X. Li, B. Horsfield, X. Tang, W.L. Jiang, Q. Chen, Energy Fuels 27 (2013) 2933–2941.
[8] H. Tian, L. Pan, X.M. Xiao, R.W.T. Wilkins, Z.P. Meng, B.J. Huang, Mar. Petrol. Geol. 48 (2013) 8–19.
[9] J.Q. Tan, P. Weniger, B. Krooss, A. Merkel, B. Horsfield, J.C. Zhang, C.J. Boreham, G. Graas, B.A. Tocher, Fuel 129 (2014) 204–218.
[10] T.T. Cao, Z.G. Song, S.B. Wang, X.X. Cao, Y. Li, J. Xia, Mar. Petrol. Geol. 61 (2015) 140–150.
[11] H. Tian, L. Pan, T.W. Zhang, X.M. Xiao, Z.P. Meng, B.J. Huang, Mar. Petrol. Geol. 62 (2015) 28–43.
[12] J.Q. Tan, B. Horsfield, N. Mahlstedt, J.C. Zhang, C.J. Boreham, D. Hippler, G. Graas, B.A. Tocher, Int. Geol. Rev. 57 (2015) 305–326.
[13] R.M. Slatt, N. O'Brien, AAPG Bull. 95 (2011) 2017–2030.
[14] G.R. Chalmers, R.M. Bustin, I.M. Power, AAPG Bull. 96 (6) (2012) 1099–1119.
[15] S. Bernard, R. Wirth, A. Schreiber, H.M. Schulz, B. Horsfield, Int. J. Coal Geol. 103 (2012) 3–11.
[16] G.R.L. Chalmers, D.J.K. Ross, R.M. Bustin, Can. Int. J. Coal Geol. 103 (2012) 120–131.
[17] J.Q. Tan, B. Horsfield, N. Mahlstedt, J.C. Zhang, R. Primio, T.A.T. Vu, C.J. Boreham, G. Graas, B.A. Tocher, Mar. Petrol. Geol. 48 (2013) 47–56.
[18] M.F. Romero-Sarmiento, J.N. Rouzaud, S. Bernard, D. Deldicque, M. Thomas, R. Littke, Org. Geochem. 71 (2014) 7–16.
[19] G.R.L. Chalmers, R.M. Bustin, Int. J. Coal Geol. 70 (1) (2007) 223–239.
[20] M. Mastalerz, A. Schimmelmann, A. Drobniak, Y.Y. Chen, AAPG Bull. 97 (10) (2013) 1621–1643.
[21] M. Thommes, K. Kaneko, A.V. Neimark, J.P. Olivier, F. Rodriguez-Reinoso, J. Rouquerol, K.S.W. Sing, Pure Appl. Chem. 87 (9–10) (2015) 1051–1069.
[22] Z.F. Ning, B. Wang, F. Yang, Y. Zwng, J. Chen, L. Zhang, Petrol. Explor. Dev. 41 (4) (2014) 492–499.
[23] R.G. Loucks, R.M. Reed, S.C. Ruppel, U. Hammes, AAPG Bull. 96 (2012) 1071–1098.
[24] C.R. Clarkson, N. Solano, R.M. Bustin, A.M.M. Bustin, G.R.L. Chalmers, L. Hec, Y.B. Melnichenko, A.P. Radliński, T.P. Blach, Fuel 103 (2013) 606–616.
[25] M.M. Labani, R. Rezaee, A. Saeedi, A.A. Hinai, West. Aust. J. Petrol. Sci. Eng. 112 (2013) 7–16.
[26] S. Brunauer, P.H. Emmett, E.J. Teller, J. Am. Chem. Soc. 60 (1938) 309–319.
[27] J.H. de Boer, B.C. Lippens, B.G. Linsen, J.C.P. Broekhoff, A. van den Heuvel, ThJ. Osinga, J. Colloid Interface Sci. 21 (1966) 405–414.
[28] M.E. Hodson, Geochim. Cosmochim. Acta 62 (1999) 3429–3435.
[29] K. Kaneko, J. Membr. Sci. 96 (1994) 59–89.
[30] J. Wloch, M. Rozwadowski, M. Lezanska, K. Erdmann, Appl. Surf. Sci. 191 (1–4) (2002) 368–374.
[31] C. Scherdel, G. Reichenauer, M. Wiener, Microporous Mesoporous Mater. 132 (2010) 572–575.
[32] M.M. Dubinin, Chem. Rev. 60 (1960) 235.
[33] E.P. Barrett, L.S. Johner, P.P. Halenda, J. Am. Chem. Soc. 73 (1951) 373–380.
[34] P.A. Webb, C. Orr, Analytical Methods in Fine Particle Technology, Micromeritics Instrument Corp, 1997.
[35] A. Vishnyakov, P.I. Ravikovitch, A.V. Neimark, Langmuir 15 (1999) 8736–8742.
[36] A. Furmann, M. Mastalerz, A. Schimmelmann, P.K. Pedersen, D. Bish, Mar. Petrol. Geol. 54 (2014) 65–81.
[37] S. Lowell, J. Shields, A. Thomas, M. Thommes, Characterization of Porous Solids and Powders: Surface Area. Porosity and Density, Springer, 2004.
[38] J. Rouquerol, P. Llewellyn, F. Rouquerol, Surf. Sci. Catal. 160 (2007) 49.
[39] J. Rouquerol, F. Rouquerol, K.S.W. Sing, P. Llewellyn, G. Maurin, Adsorption by Powders and Porous Solids: Principles, Methodology and Applications, Academic Press, 2014.
[40] J. Landers, G.Y. Gor, A.V. Neimark, Colloids Sur. A Physicochem. Eng. Aspects 437 (2013) 3–32.
[41] Z.D. Li, Z.H. Jin, A. Firoozabadi, SPE J. 19 (6) (2014) 1096–1109.
[42] M. Thommes, K.A. Cychosz, Adsorption 20 (2014) 233–250.
[43] W.D. Harkins, G. Jura, J. Am. Chem. Soc. 66 (1944) 1366–1373.
[44] U. Kuila, M. Prasad, Geophys. Prospect 61 (2013) 341–362.